JACS
JOURNAL OF THE AMERICAN CHEMICAL SOCIETY
pubs.acs.org/JACS
Article

Disentangling Chromophore States in a Reversibly Switchable Green Fluorescent Protein: Mechanistic Insights from NMR Spectroscopy

Nina Eleni Christou, Karine Giandoreggio-Barranco, Isabel Ayala, Oleksandr Glushonkov, Virgile Adam, Dominique Bourgeois, and Bernhard Brutscher*

Cite This: https://doi.org/10.1021/jacs.1c02442
Read Online

ABSTRACT: The photophysical properties of fluorescent proteins, including phototransformable variants used in advanced microscopy applications, are influenced by the environmental conditions in which they are expressed and used. Rational design of improved fluorescent protein markers requires a better understanding of these environmental effects. We demonstrate here that solution NMR spectroscopy can detect subtle changes in the chemical structure, conformation, and dynamics of the photoactive chromophore moiety with atomic resolution, providing such mechanistic information. Studying rsFolder, a reversibly switchable green fluorescent protein, we have identified four distinct configurations of its *p*-HBI chromophore, corresponding to the *cis* and *trans* isomers, with each one either protonated (neutral) or deprotonated (anionic) at the benzylidene ring. The relative populations and interconversion kinetics of these chromophore species depend on sample pH and buffer composition that alter in a complex way the strength of H-bonds that contribute in stabilizing the chromophore within the protein scaffold. We show in particular the important role of histidine-149 in stabilizing the neutral *trans* chromophore at intermediate pH values, leading to ground-state *cis*−*trans* isomerization with a peculiar pH dependence. We discuss the potential implications of our findings on the pH dependence of the photoswitching contrast, a critical parameter in nanoscopy applications.

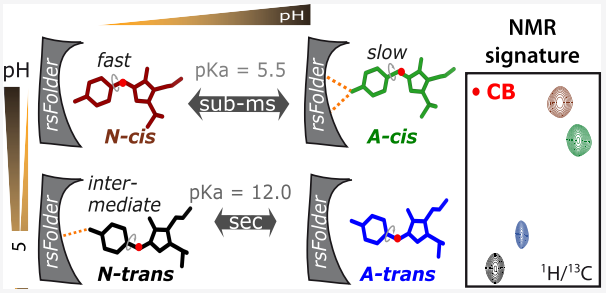

INTRODUCTION

Phototransformable fluorescent proteins (PTFPs) change their fluorescent state upon illumination at specific wavelengths and are thus crucial for a wide range of applications in advanced fluorescence microscopy[1−3] and biotechnology.[4,5] In this study, we focus on reversibly switchable fluorescent proteins (RSPFs) of the green fluorescent protein (GFP) family that can be reversibly photoswitched between a fluorescent on-state and a nonfluorescent off- state. Depending on whether the wavelength that excites fluorescence switches the RSFP from the on- to off-state, or vice versa, RSFPs are said to be negative or positive, respectively.[6] In the absence of light, the metastable off-state (or on-state) spontaneously converts back to the thermodynamically stable on-state (or off-state) on a time scale ranging from seconds to hours. A large number of RSFPs have been engineered from both hydrozoan and anthozoan fluorescent protein sequences.[6−11] All of them share a common 11-stranded β-barrel fold, enclosing an endogenous 4-(*p*-hydroxybenzylidene)-5-imidazolinone (*p*-HBI) chromophore formed by a Xxx-Tyr-Gly tripeptide (where Xxx is a variable amino acid). During protein folding, in the presence of oxygen, this tripeptide autocatalytically transforms into a conjugated π-electron system consisting of two aromatic rings connected by a methine bridge. In solution, the isolated *p*-HBI chromophore can freely rotate around the P and I bonds of the methine bridge, which makes it nonfluorescent due to nonradiative de-excitation pathways.[12−15] In GFPs, however, the chromophore is anchored to the protein scaffold in the center of the β-barrel by two short helices as well as additional H-bonding, electrostatic, and van der Waals interactions with neighboring amino acids. This reduces the conformational flexibility of the chromophore, resulting in an up to 3 orders of magnitude increased fluorescence quantum yield (QY) compared to the same chromophore in solution.[12,16] Even slight changes in the chromophore's local environment can significantly alter the photophysical properties of a RSFP, such as fluorescence quantum yield, photoswitching kinetics, and photoswitching contrast.[17] Understanding the relationship between changes in the chromophore's local environment, induced either by environmental physicochemical conditions

Received: March 8, 2021

or by mutations, and the observed photophysical properties is therefore of utmost importance for rational engineering of robust RSFP variants optimized for particular applications.

X-ray crystal structures solved at cryogenic temperatures for a number of RSFPs[6,11,18] have shown that the chromophore is generally found in a *cis* (or *Z*) configuration in the fluorescent on-state, while it adopts predominantly a *trans* (or *E*) configuration in the light-induced nonfluorescent off-state (an exception is the negative RSFP rsGamillus, where the chromophore adopts a *trans* configuration in the fluorescent on-state[19]). Except for rare cases,[20] the resolution of these X-ray structures is not sufficient to observe the position of hydrogen atoms. Therefore, the protonation state of the chromophore and surrounding titrating residues has to be inferred from steric hindrance arguments, often leading to ambiguities. Additional information about the chromophore's protonation state can be obtained from optical methods, such as UV−vis or vibrational spectroscopy. These optical methods, however, are only poorly sensitive to *cis*−*trans* isomerization, making it challenging to disentangle *cis*−*trans* isomerization from protonation/deprotonation events.[17,21,22] Protonation/deprotonation events of the chromophore and surrounding residues as well as subsequent hydrogen bond formation and breakage play a major role in the relative stability of different chromophore configurational states and the energy barriers between them. X-ray structures solved at cryogenic temperatures also lack information about the presence of multiple conformations that are in conformational exchange at various time scales.

High-field multidimensional solution nuclear magnetic resonance (NMR) spectroscopy is a particularly powerful tool to investigate at atomic resolution the conformational dynamics of proteins under different environmental conditions. In particular, NMR chemical shifts are sensitive to protonation/deprotonation events and the formation of hydrogen bonds, both being influenced by pH and buffer composition. We have chosen rsFolder[11] as a model protein for a negative RSFP for our NMR study. X-ray crystal structures of rsFolder in the dark-adapted on-states and light-induced off-states revealed a change in the chromophore configuration from *cis* (fluorescent on-state) to *trans* (nonfluorescent off-state). Recently, we have reported NMR assignments (^{1}H, ^{13}C, and ^{15}N) of rsFolder in both the on- and off-states at physiological pH.[23] It was assumed that the chromophore in the on- and off-states was in an anionic *cis* and a neutral *trans* configuration, respectively. Here, we show that NMR spectroscopy has the resolving power to spectrally distinguish four different chromophore species, allowing accurate quantification of state populations under various sample conditions (pH and buffer composition) as well as providing information about the conformational dynamics of the chromophore and surrounding residues in each state and the exchange kinetics between them. We demonstrate the occurrence of significant pH-induced ground-state chromophore isomerization in this negative green RSFP, even in the absence of light illumination. We also observe a complex pH-dependent stabilization of the *trans* chromophore and propose a mechanistic model that accounts for it. We discuss implications of our findings on the pH dependence of the photoswitching contrast, a critical parameter in nanoscopy approaches.[24]

RESULTS AND DISCUSSION

NMR Spectral Signatures of Chromophore Configurations. The *p*-HBI chromophore can adopt two (main) protonation states with the hydroxyphenyl moiety either protonated at the phenolic oxygen (neutral species, N) or deprotonated (anionic species, A). In addition, the chromophore can undergo *cis*−*trans* isomerization around the imidazolinone bond (I-bond), yielding a total of at least four potentially populated chromophore states, as shown in Figure 1.

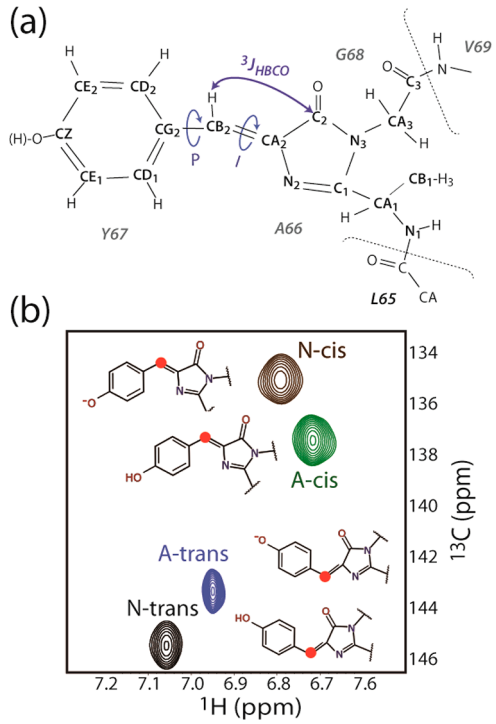

Figure 1. (a) Chemical structure and atom nomenclature of the*p*-HBI chromophore formed by the tripeptide A66-Y67-G68. The phenoxy (P) and imidazolinone (I) bonds of the methine bridge are indicated. The three-bond scalar coupling constant $^{3}J_{HBCO}$ is sensitive to I-bond rotations, allowing to differentiate between *cis* and *trans* isomers. (b) Characteristic NMR signature of the chromophore CB_2−H pair (position highlighted in red on *p*-HBI structure) in the four configurational chromophore states: A-*trans*, A-*cis*, N-*trans*, and N-*cis*. Superposition of NMR signals recorded under different pH and illumination conditions: no illumination at pH 8 (green), no illumination at pH 4.5 (brown), 488 nm illumination at pH 8 (black), and 488 nm illumination at pH 11.5 (blue).

Interestingly, we found that the C_β carbon (CB_2) of the chromophore's methine bridge exhibits a large ^{13}C chemical shift change ($\Delta\delta$ = 7.6 ppm) upon photoswitching. The two correlation peaks observed at pH 7.5 in the on- and off-states were assigned to the A-*cis* and N-*trans* configurations of the chromophore, respectively. At low pH (4.5), the NMR signature of the CB_2−H pair in the off-state remains unchanged, while the on-state CB_2−H peak is detected at a different position, tentatively assigned to the N-*cis* configuration (Figure S1a). At very high pH (11.5), two correlation peaks are detected for the CB_2−H of the chromophore methine bridge under 488 nm light illumination (off-state), with the additional peak most likely arising from the A-*trans* species. It has been reported that $^{3}J_{HBCO}$ coupling constants

https://doi.org/10.1021/jacs.1c02442
J. Am. Chem. Soc. XXXX, XXX, XXX−XXX

(Figure 1a) of synthetic *p*-HBI chromophore analogues are sensitive reporters of *cis*−*trans* isomerization of the I-bond.[25,26] NMR measurements of $^{3}J_{HBCO}$ coupling constants of rsFolder chromophore are in agreement with our assignment of these peaks, with values of ∼10 Hz for the *trans* configuration and ∼5 Hz for the *cis* configuration. Also, the ^{1}H chemical shifts are in good qualitative agreement with those measured for isolated model GFP chromophores.[25] The CB_2−H correlation thus provides a convenient NMR signature (Figure 1b) for identifying the different chromophore species under a set of experimental conditions.

Similar NMR spectral signatures, characteristic of the four chromophore configurational states, are also observed for other protein backbone and side-chain nuclei that are in spatial proximity to the chromophore (Figure S1b). Of particular note is that chromophore *cis*−*trans* isomerization can cause significant chemical shift changes for nuclei, e.g., H−N pairs, far away from the chromophore (due to ring current shift effects). Therefore, measuring NMR peak intensities for nuclear sites that experience a strong chemical shift change upon chromophore isomerization, but that are only little affected by NMR line broadening, induced by exchange dynamics in the chromophore pocket allows accurate quantification of chromophore state populations.

***Cis* Chromophore Protonation Equilibrium and Ring-Flip Dynamics.** The relative populations of neutral and anionic chromophore species can be varied by adjusting the H^+ concentration in the solvent (pH). 2D ^{1}H−^{13}C correlation spectra were recorded for a series of rsFolder samples in McIlvaine buffers (MI, mixture of disodium phosphate and citric acid), adjusted to pH values ranging from 4.2 to 8.0 (4.2 corresponding to the lowest pH value at which rsFolder does not show signs of protein unfolding over the NMR measurement time of several hours). These data revealed that the chromophore's CB_2−H correlation peak is progressively shifting from the A-*cis* to the N-*cis* position when the pH is lowered (Figure 2b). The same behavior is observed for NMR signals of several side-chain and amide backbone nuclei close to the chromophore in the *β*-barrel structure (Figure 2a). The observed peak shifts are indicative of fast chromophore protonation/deprotonation exchange kinetics with an exchange rate constant $k_{ex} = (k_{prot} + k_{deprot}) \gg 1000\ s^{-1}$ over the entire pH range. This observation suggests that solvent hydrogens can easily migrate into the *β*-barrel and protonate the hydroxybenzylidene ring of the *cis*- chromophore on a sub-milliseconds time scale. The pH-induced chemical shift variations measured for a total of 12 nuclei fit well to a simple bimolecular reaction as described by the Henderson−Hasselbalch equation with an apparent pK_a value of pK_{cis} = 5.45 ± 0.05 and a Hill coefficient of 1 (Figure 2c and Figure S2). NMR spectra recorded for rsFolder dissolved in a phosphate-free HEPES buffer at pH 6 reveal increased line broadening for nuclei that show pH-induced peak shifts compared to spectra recorded in the phosphate-containing MI buffer (Figure 2d). It is well-known that phosphate ions can catalyze proton transfer reactions,[27−30] and indeed, when phosphate is added to the HEPES buffer, the spectral intensities observed in MI buffer are restored (Figure S3). These observations can be explained by slower protonation/deprotonation exchange kinetics in the absence of phosphate in the sample solution, shifting the kinetic time scale to the intermediate exchange regime ($k_{ex} \approx 1000\ s^{-1}$), responsible for the observed NMR line broadening. To further quantify the exchange dynamics underlying the observed line broadening, we have performed ^{15}N Carr−Purcell−Meiboom−Gill

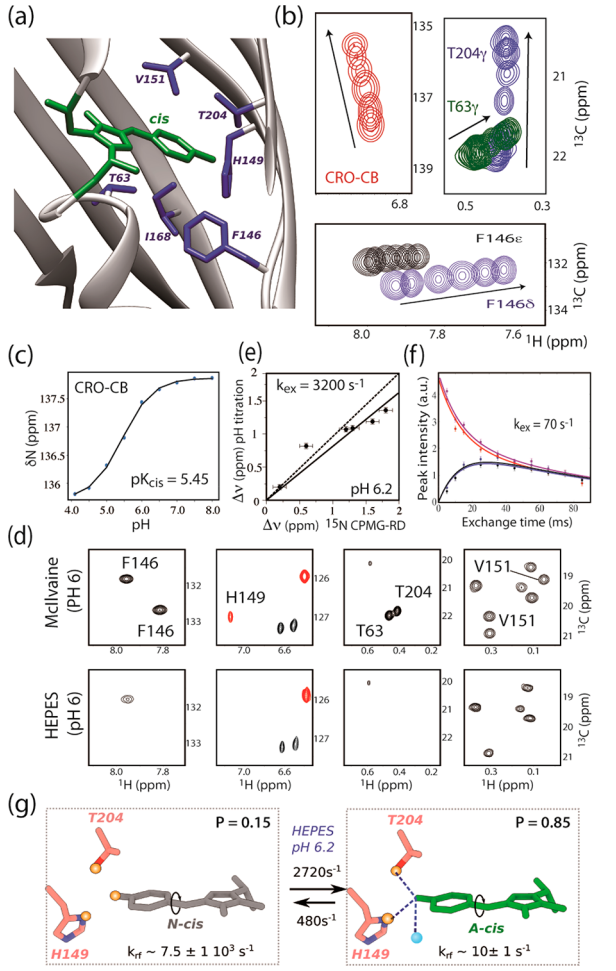

Figure 2. pH dependence of *cis* chromophore protonation and dynamics. (a) Zoom on the *cis* chromophore environment extracted from the X-ray structure of rsFolder on-state (PDB: 5DTZ).[11] Side chains with nuclei that show large pH-dependent chemical shift changes are highlighted in blue. (b) pH-titration effects observed in the NMR spectra for the CB_2−H of the methine bridge and other nuclei close to the chromophore. Six spectra recorded in the pH range from 7.5 to 4.2 (as indicated by an arrow) are superposed and color-coded to distinguish different nuclear sites. (c) Fit of the observed chemical shift variations to a bimolecular reaction as described by the Henderson−Hasselbalch equation with a pK_a of 5.45. (d) Spectral differences in the aromatic and methyl regions of ^{1}H−^{13}C correlation spectra of rsFolder (850 MHz, 40 °C) in the dark-adapted on-state at pH 6 induced by a different buffer medium: MI buffer (top panel) or HEPES buffer (bottom panel). Red peaks are detected with negative signal intensity due to constant-time ^{13}C frequency editing. (e) Linear correlation of chemical shift differences extracted from the pH titration series and ^{15}N CPMG-RD data. A correlation coefficient of 0.95 between the two data sets is obtained for linear regression with a slope of m = 0.82 (straight line), supporting our exchange model. Note that the deviation from m = 1 (dashed line) may be easily rationalized by a slight miscalibration of the sample pH (about 0.1 pH units). (f) Numerical fit of EXSY NMR data recorded for the CE sites of the hydroxybenzylidine ring at pH 7.5 providing an estimate of the ring flip rate around the P-bond. (g) Graphical sketch summarizing the major findings on the (de)protonation kinetics, ring-flip dynamics, and H-bond stabilization of the *cis* chromophore in rsFolder. Yellow and blue balls represent hydrogen atoms and water molecules, respectively.

https://doi.org/10.1021/jacs.1c02442
J. Am. Chem. Soc. XXXX, XXX, XXX−XXX

(CPMG) relaxation-dispersion (RD) NMR measurements.[27,28] ^{15}N CPMG-RD data contain information about the lifetimes of the exchanging states, their relative populations, and the chemical shift differences between them. The ^{15}N CPMG-RD data obtained for six amide sites of rsFolder at two different magnetic field strengths are plotted in Figure S4. For data fitting, we assumed a two-state (A-*cis* and N-*cis*) exchange model with the respective populations at pH 6.2 equal to 0.85 (A-*cis*) and 0.15 (N-*cis*), as deduced from the Henderson−Hasselbalch equation with the pK_{cis} = 5.45. A global fit of the CPMG-RD data to this exchange model leads to an excellent agreement between measured and back-calculated data for an exchange rate constant k_{ex} = 3200 ± 200 s^{-1}. This result indicates that the NMR line broadening observed for the six amide sites is caused by a single kinetic process, i.e., the exchange of the anionic and neutral *cis* chromophore states. To further validate this assumption, we compared the ^{15}N chemical shift changes extracted from the pH titration series (Figure S2) with those obtained from fitting the ^{15}N CPMG-RD dispersion data (Figure S4), resulting in the correlation plot shown in Figure 2e.

Protonation and deprotonation of the *cis* chromophore in rsFolder are substantially accelerated by the presence of phosphate ions. Although molecular dynamics simulations indicate that small molecules such as oxygen may penetrate within the β-barrel of fluorescent proteins,[29,30] it remains unclear whether phosphate can diffuse toward the rsFolder chromophore's phenyl moiety at a sufficiently fast rate. pH-jump studies of the green fluorescent protein EGFP[31,32] have shown that the rate-limiting step of *cis* chromophore (de)protonation is the transfer of protons through the protein matrix via a network of proton acceptors and donors.[32−34] Thus, the observed increased (de)protonation exchange rate is more likely explained by a raise in proton shuttling efficiency at the accessible protein surface due to the catalytic action of phosphate ions.

The *cis* chromophore can rotate around the phenoxy (P) bond of the methine bridge, leading to aromatic ring flips. Ring flip rates for solvent-exposed tyrosine side chains on the order of 10^3−10^5 s^{-1} have been reported at ambient temperature.[35] For rsFolder, distinct NMR signals are detected for the CD and CE sites of the hydroxybenzylidine ring at 40 °C and high pH (≥7), indicating slow ring flip dynamics in the A-*cis* state under these conditions. With decreasing pH, these NMR signals strongly line broaden or even completely disappear from the spectra when the apparent ring-flip rate, resulting from the population-weighted average of the A-*cis* and N-*cis* ring flips, becomes comparable to the chemical shift difference of the two magnetically equivalent sites ($\omega_{CD1} - \omega_{CD2}$ or $\omega_{CE1} - \omega_{CE2}$). At low pH (≤5.5), a single peak is detected for the CE position (Figure S5a), while the CD site remains unobserved due to the larger chemical shift difference between ω_{CD1} and ω_{CD2}.

In the slow exchange regime, observed at high pH, the ring flip kinetics can be further quantified by 2D exchange spectroscopy (EXSY)[36] which monitors the intensity buildup of cross-peaks correlating the ^{13}C frequency of one site with the ^{1}H frequency of the second site (Figure 2f and Figure S5b). We have measured the ring flip rate k_{rf} of the *cis* chromophore at three different pH values by using such an EXSY experiment (Figure S5c), resulting in exchange rate constants $k_{ex} = 2k_{rf}$ of 26 ± 2 s^{-1} (pH 10.7), 70 ± 5 s^{-1} (pH 7.5), and 230 ± 50 s^{-1} (pH 7.2). In addition, the observed coalescence (extreme line broadening) of the two CE−HE correlation peaks at about pH 6 allows to estimate the exchange rate at this particular pH to be $k_{ex} \approx 1/(2\pi\Delta\nu)$ = 3500 s^{-1}. As expected, the ring flip rate increases with decreasing pH as a consequence of N-*cis* becoming more populated. Individual ring-flip rates of the A-*cis* and N-*cis* states were obtained by fitting the measured data to a Henderson−Hasselbalch equation with a pK_a of 5.45, describing the population average of the two states (Figure S5d). Our data demonstrate that the P-bond in the A-*cis* state is very rigid with a ring-flip rate of only 10 ± 1 s^{-1} at 40 °C, while the flexibility of the P-bond in the N-*cis* state, with an extrapolated rate constant k_{rf} = (7.5 ± 0.1) × 10^3 s^{-1}, is comparable to a free chromophore in solution. This finding provides a plausible explanation for the nonfluorescence of the N-*cis* state upon absorption at 405 nm, which may apply to many GFPs when no excited-state proton transfer occurs.

Role of H149 in Proton Transfer. H149 has been shown to be a critical residue in the photoswitching mechanism of rsEGFP2, notably involved in chromophore deprotonation upon *trans*−*cis* isomerization.[37] Our crystallographic[11] and NMR[23] data indicate that in rsFolder H149 (ND_1) is forming a hydrogen bond with the phenolate ring of the anionic A-*cis* chromophore. With increasing population of the neutral N-*cis* configuration, the ND_1−H NMR signal observed at high pH is no longer detected at lower pH (Figure S6a). This confirms that this H-bond is constantly breaking and re-forming as a consequence of proton exchange at the chromophore hydroxybenzylidene ring. Our NMR data also provide valid information about the tautomeric state of the histidine ring after protonation of the *cis* chromophore. While the CE_1 is a sensitive reporter of the charge state of the imidazole ring (neutral or cationic), the CD_2 and CG chemical shifts report on its tautomeric state: ND_1−H or NE_2−H (Figure S6b). The CE_1, CG, and CD_2 frequencies of H149 are only slightly changing between the A-*cis* (high pH) and N-*cis* (low pH) conformations (Figure S6c), indicating that the average charge and tautomeric state populations are only little altered by the proton transfer reaction. H149 remains predominantly in a ND_1−H tautomeric configuration. Consequently, if H149 is the proton donor of the *cis* chromophore, it has to be part of a more extended protonation chain, allowing the imidazole ring to become quickly reprotonated at the $N_{\delta1}$ position, in agreement with previous proposals on EGFP.[33,38]

The graphical sketch in Figure 2g summarizes our NMR findings about the protonation kinetics, conformational dynamics, and hydrogen bonding of the *cis* chromophore in rsFolder.

***Trans* Chromophore Protonation Equilibria and Ring-Flip Dynamics.** In the off-state of rsFolder, no significant changes of NMR chemical shifts are observed for the CB_2−H moiety of the chromophore and nuclei of surrounding residues in the pH range 4.5−11.5 (Figure 3 and Figure S1). However, an additional NMR signal, assigned to an A-*trans* chromophore configuration, is detected at pH 11.5. This is in agreement with the pK_a of the *trans* chromophore (de)protonation equilibrium being shifted to high pH (>10), as reported for other RSFPs.[39] Assuming a simple bimolecular process, we can estimate the pK_a from the N-*trans* and A-*trans* populations measured at pH 11.5 to be pK_{trans} = 12.0 ± 0.1 in rsFolder. This pK_a is ∼3 pH units higher than what is observed for a hydroxyphenyl ring in aqueous solution.[40] Contrary to the situation observed for the *cis* chromophore in rsFolder, where the NMR signals of nuclei

https://doi.org/10.1021/jacs.1c02442
J. Am. Chem. Soc. XXXX, XXX, XXX−XXX

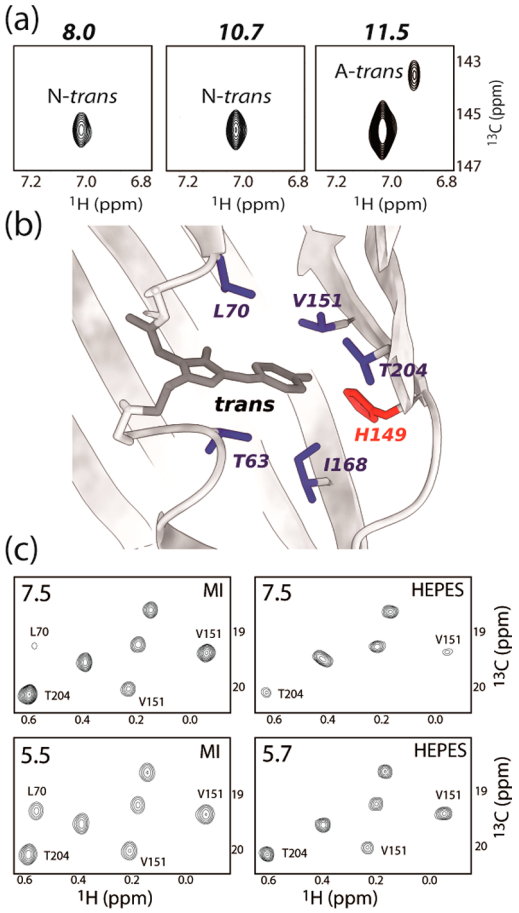

Figure 3. (a) NMR signature of the chromophore's CB_2−H moiety in the *trans* configuration, recorded under 488 nm illumination at 40 °C for different pH values. The observed peaks are annotated. (b) Zoom-in on the *trans* chromophore environment extracted from the X-ray structure of rsFolder off-state (PDB: 5DU0).[11] Side chains with nuclei that show pH- and buffer-dependent line broadening in the methyl spectra shown in (c) are highlighted in blue, while H149 at the origin of this NMR line broadening is color-coded in red. (c) Methyl region of $^1H-^{13}C$ correlation spectra, recorded under 488 nm illumination at 40 °C for different pH values (as indicated) and buffer conditions (MI or HEPES). The slight difference in the acidic pH values for HEPES and MI is insignificant for our conclusions.

in the proximity of the chromophore shift as a function of pH, two distinct peaks are detected for rsFolder in the *trans* chromophore isomeric state, indicative of proton exchange kinetics $k_{ex} \ll 1000\ s^{-1}$. Proton transfer to/from the rsFolder *trans* chromophore is thus a much slower process than what is observed for the rsFolder *cis* chromophore, a consequence of the absence of efficient proton transfer pathways that allow to quickly evacuate a proton from the hydroxyphenyl ring to the bulk water.

No NMR signals could be detected for the symmetrical CD and CE sites of the hydroxybenzylidine ring of the *trans* chromophore independent of pH and buffer composition. This indicates that the P-bond in the N-*trans* state is rotating at an intermediate flip rate that we can estimate (from the *cis* chromophore chemical shifts) to be in the range $k_{rf} \approx 300-1000\ s^{-1}$ or undergoes different types of millisecond time scale motion inside the β-barrel.

In our recent NMR study,[23] we could show that the chromophore pocket and parts of the β-barrel in the N-*trans* state of rsFolder in HEPES buffer at pH 7.5 are dynamic with conformational substates interconverting on the millisecond time scale, as inferred from extensive NMR line broadening observed for backbone and side chain resonances close to the chromophore (Figure 3b). Interestingly, these line broadening effects are pH and buffer dependent. In particular, they are considerably reduced when replacing the organic HEPES buffer with a phosphate-containing MI buffer or by lowering the pH (Figure 3c). These observations indicate that the conformational dynamics underlying the NMR line broadening are related to a second (de)protonation event in the chromophore pocket, different from the protonation of the chromophore's phenyl ring. As will be discussed in more detail below, the most likely candidate titrating in the pH range 5.5–7.5 is the imidazoline ring of H149.

Thermodynamics and Kinetics of *Cis*–*Trans* Chromophore Isomerization in the Dark. Quantitative information about the free-energy difference between the *cis* and *trans* chromophore configurations in rsFolder is obtained from NMR measurements of state populations. The *trans* chromophore population calculated from CB_2−H peak intensities, measured in $^1H-^{13}C$ correlation spectra (Figure S7a) as a function of pH, is plotted in Figure 4a. The *p*-HBI chromophore in rsFolder undergoes pH-induced *cis*–*trans* isomerization, with the population of the *trans* configuration increasing at lower pH values and reaching a maximum value

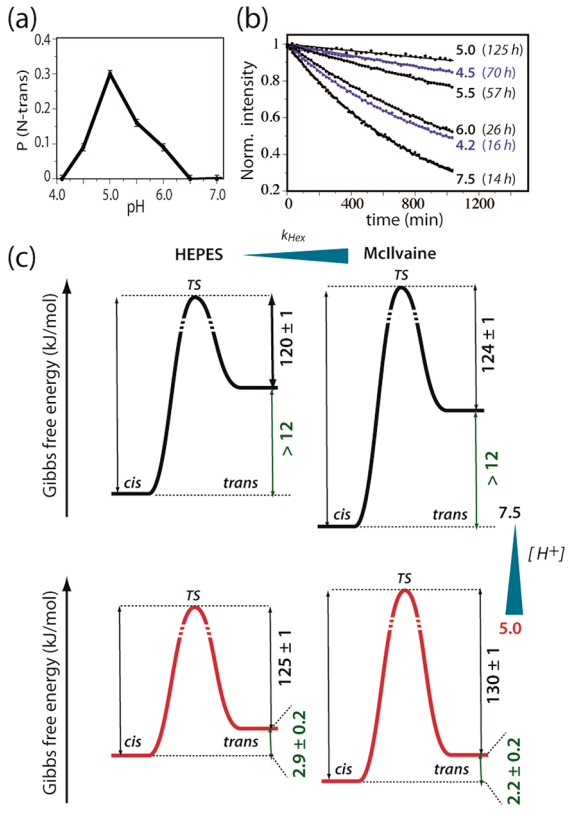

Figure 4. (a) N-*trans* population measured as a function of pH from the CB2-H peak intensities in the absence of light. (b) Normalized thermal relaxation kinetics observed for rsFolder in MI buffer at different pH values. For better visibility, data for pH < 5.0 are plotted in blue. (c) Energy landscape of *cis*–*trans* isomerization in rsFolder derived from the NMR data shown in (a) and (b) for different pH (black: 7.5; red: 5.0) and buffer composition (left: HEPES; right: MI).

https://doi.org/10.1021/jacs.1c02442
J. Am. Chem. Soc. XXXX, XXX, XXX−XXX

of 30% at pH 5.0. At even lower pH, the *trans* chromophore configuration decreases again and is no longer detected at pH 4.2. The same pH-dependent behavior is observed for amide backbone $^{1}H-^{15}N$ correlations that show significant chemical shift changes upon *cis*−*trans* chromophore isomerization (Figure S7b). pH-induced chromophore *cis*−*trans* isomerization in the electronic ground state has been previously observed in nonreversibly photoswitchable fluorescent proteins such as mKate[41] and mKeima.[42] However, for these proteins, a complete switch of isomeric state is observed at low pH relative to high pH, while a mixed population between *cis* and *trans* configurations of the chromophore is observed at intermediate pH values. The partial occupancy of the *trans* isomeric state at around pH 5.0 is thus (so far) unique to rsFolder. Its mechanistic interpretation is most likely related to the presence of a titrable residue in the immediate vicinity of the chromophore changing its protonation state with a pK_a close to pH 5.

The pH-dependent buildup of N-*trans* species in the dark has also implications for the apparent pK_a obtained from fluorescence or absorbance measurements. While NMR chemical shifts report on the pK_a of chromophore protonation/deprotonation in the pure isomeric *cis*-state, optical measurements typically probe the amount of the fluorescent A-*cis* species as a function of pH, which results from the combined effect of protonation, as well as *cis*−*trans* isomerization (Figure S8).

Additional information about the free energy landscape of rsFolder *cis*−*trans* isomerization is obtained from thermal relaxation measurements. The *trans* chromophore can be populated to a high level by 488 nm sample illumination. In the dark, this light-induced *trans* chromophore population spontaneously reconverts to the *cis* chromophore configuration until reaching a thermodynamic equilibrium. Thermal relaxation kinetics can be accurately quantified by measuring the intensity decay or buildup of NMR signals characteristic for one of the two states. Figure 4b shows our NMR results of *trans*-to-*cis* interconversion measurements at 40 °C for a range of rsFolder samples in MI buffers at different pH values. The observed pH dependence of thermal relaxation times is similar to what we reported in Figure 4a for the *trans* chromophore population: the thermal relaxation time increases from 14 h at pH 7.5 to a maximum of 125 h at pH 5.0, before decreasing again to 16 h at pH 4.2. To derive energy barriers between the *trans* chromophore state and the transition state(s) along the pathway to the *cis* chromophore state, we have measured the temperature dependence of thermal relaxation at pH 7.5 in HEPES buffer. Using an Arrhenius relation, we determined the activation energy for *trans*-to-*cis* conversion in the dark to be 120 ± 5 kJ/mol under these conditions (Figure S9). We have also remeasured some NMR data (pH 7.5 and 5.0) in HEPES buffer (Figure S10) to evaluate the influence of buffer composition, and in particular the presence of phosphate ions, on the energetic landscape of *cis*−*trans* isomerization. The resulting free energy landscapes for MI and HEPES buffer at pH 7.5 and 5.0, assuming a two-state exchange process with a single activation energy barrier, are shown in Figure 4c. Our NMR-derived energy landscapes do not provide absolute values for the free energies of the *cis* and *trans* chromophore states but only information about activation energies (energy difference between the ground and transition state). Therefore, the observation of a reduced activation energy may be explained by either higher energy of the ground state, or lower energy of the transition state, or both.

Concerning the *cis* chromophore, we observe a reduction in activation energy at low pH, which may be ascribed to an increasing amount of N-*cis* population (<1% at pH 7.5 vs 74% at pH 5). The observed energy difference is thus mainly due to enthalpic stabilization of the A-*cis* chromophore by H-bonding to the β-barrel that is lost after protonation of the chromophore's hydroxyphenyl moiety. In contrast, in the case of the *trans* chromophore, our data indicate a higher activation energy at pH 5.0, which we relate to the data in Figure 4a which suggest a stabilization of the rsFolder *trans* chromophore state at this pH.

Interestingly, in both directions, we observe that the activation energy for chromophore isomerization in the electronic ground state is decreased in a HEPES buffer as compared to a MI buffer, that is, if the proton exchange kinetics are slowed down. We currently do not have a clear explanation for this observation, which may however be tentatively ascribed to a destabilization of the transition state(s) between the *cis* and *trans* conformational states.

Potential Role of H149 in *trans* Chromophore Stabilization at pH 5. We do not have direct evidence of what is causing the apparent *trans* chromophore stabilization at pH 5.0, but we speculate that hydrogen bonding of the hydroxyl group of the chromophore with the imidazoline ring of H149 is the main driving force. Such H-bond formation has been observed at low-temperature in the X-ray structure of rsFolder in its off-state.[11] To be a proton acceptor, the H149 side chain has to be in a neutral state, i.e., protonated only on one of the ring nitrogens. As discussed above, NMR provides a valuable tool to infer the tautomeric and charge state of histidine side chains. The $CE_1(H)$ frequencies of H149 are only slightly changed after chromophore isomerization, indicating that the imidazoline ring remains predominantly neutral at pH > 5. Furthermore, we could not detect any NMR signal for the CD_2 and CG sites, which are sensitive to the tautomeric state, over the entire sampled pH range. This may be explained by extensive NMR line broadening due to the interconversion of ND_1-H and NE_2-H tautomeric states at the millisecond time scale. At pH 5.0 and/or in the presence of phosphate ions, we observe NMR line narrowing for nuclei close to H149 (Figure 3c). This can be ascribed to accelerated exchange kinetics, as confirmed by the temperature dependence of the observed line broadening effects (Figure S11a), shifting the exchange kinetics out of the intermediate NMR exchange regime for nuclear sites with relatively small chemical shift differences between the two states. The expected large chemical shift differences for the CD_2 (4 ppm) and CG (9 ppm) of the H149 side chain (Figure S6b) explain why these resonances remain unobserved in our NMR spectra. Furthermore, we hypothesize that the equilibrium is shifted toward the NE_2-H tautomeric state at pH 5.0, favoring H-bond formation with the chromophore, as illustrated in Figure 5.

This population shift is supported by small chemical shift changes observed in the off-state of rsFolder for some of the side chain nuclei in the vicinity of H149 in the pH range between 5.0 and 7.5 (Figure S11b). The ∼5−6 kJ/mol difference observed between the activation energies of the *trans* chromophore state at pH 7.5 and 5.0 is within the reported range of hydrogen-bond formation in proteins[43,44] and therefore further supports our model of stabilization of a

https://doi.org/10.1021/jacs.1c02442
J. Am. Chem. Soc. XXXX, XXX, XXX−XXX

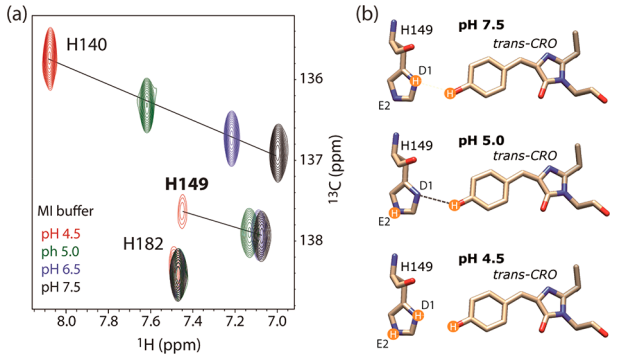

Figure 5. (a) Spectral overlay of color-coded $^{1}H-^{13}C$ correlation spectra, highlighting the different titration behavior of three histidine CE_1-H side-chain resonances as a function of pH. While H182 remains in a neutral tautomeric state over the whole pH range, H140 is titrating like a free histidine in solution with a pK_a of ~6.5, and H149 only starts shifting significantly below pH 5. (b) During pH titration, the relative populations of H149 tautomeric states shift from predominantly ND_1-protonated (high pH), NE_2-protonated (pH 5), to biprotonated (low pH). Only the NE_2-protonated tautomer can form a H-bond with the protonated chromophore.

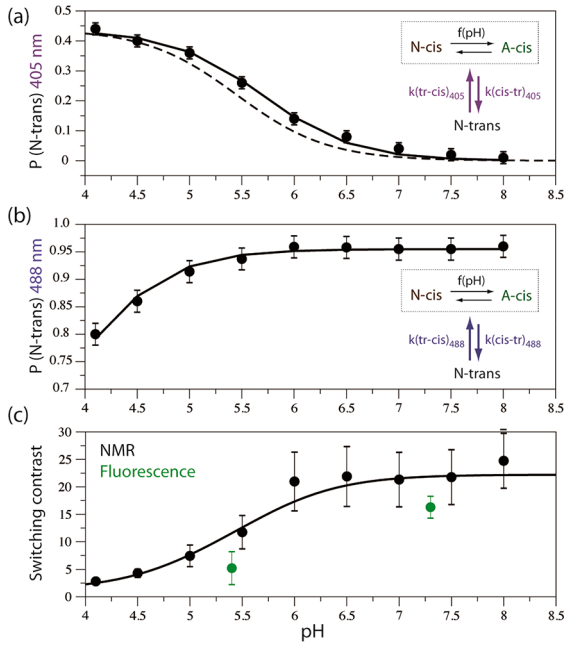

Figure 6. NMR measurements of the pH dependence of N-*trans* chromophore populations in rsFolder under continuous (a) 405 nm and (b) 488 nm light illumination. The straight lines are fits of the experimental data to a Henderson–Hasselbalch relation, while the dashed line in (a) is the calculated behavior for a pK_a of 5.45. A kinetic model is shown in the inset. (c) NMR-derived switching contrast (black points), calculated as $P(A\text{-}cis)_{405}/(P(A\text{-}cis)_{488}$. In addition, the switching contrast measured by fluorescence microscopy on protein samples in highly concentrated MI buffers at two pH values, and fixed in polyacrylamide gels, is plotted as green dots. The lower contrast observed by fluorescence microscopy as compared to NMR may be due to differences in sample conditions.

single H-bond between the hydroxyl group of the chromophore and the imidazoline ring of H149.

At pH < 5, a cationic form of H149 becomes increasingly populated as deduced from characteristic CE_1-H frequency shifts observed at low pH (Figure 5a). The doubly protonated histidine side chain is no longer able to form a H-bond with the N-*trans* chromophore, thus explaining the energetic destabilization of the *trans*-CRO under such acidic conditions.

Chromophore State Populations under Light Illumination and Switching Contrast. To investigate the consequences of the observed pH-induced ground-state free energy changes for photoswitching nanoscopy techniques such as reversible saturable optical fluorescence transition (RESOLFT) microscopy, we also measured chromophore state populations under light illumination conditions.

Figure 6 shows NMR-derived N-*trans* populations under continuous (a) 405 nm and (b) 488 nm illumination as a function of pH. To analyze these data, we assume a simple kinetic model as depicted in the insets of Figures 6a and 6b. The steady-state population reached at each pH is governed by the relative photoswitching rates at a particular wavelength between the A/N-*cis* and the N-*trans* isomeric states and by the pH-dependent equilibrium of N-*cis* and A-*cis* populations. The latter assumption is supported by the fact that NMR on-state peak positions are not affected by illumination at either wavelength. The kinetic rate constants are given by the population-weighted (in the case of the *cis* chromophore) product of the extinction coefficient (ε_{cis} or ε_{trans}) of the *cis* or *trans* states at the actinic wavelength (405 or 488 nm) and the respective switching quantum yield (QY(tr-cis) or QY(cis-tr)). In the case of pH-independent extinction coefficients and switching QY of the different chromophore species, the N-*trans* population is expected to follow a Henderson–Hasselbalch relation with the pK_a of the *cis* chromophore (5.45), as derived from our ground-state NMR data.

Under 405 nm illumination (Figure 6a) and high pH, the measured N-*trans* population is close to zero, indicating that the A-*cis* chromophore (populated at close to 100%) is not able to switch and that the switching rate $k(\text{cis-tr})_{405}$ is solely determined by the properties (extinction coefficient and switching quantum yield) of N-*cis*. At pH < 4.0, a N-*trans* population of about 0.45 ± 0.05 is observed which translates to comparable switching rates in both directions ($k(\text{cis-tr})_{405} \approx k(\text{tr-cis})_{405}$). In other words, at acidic pH the extinction coefficients and switching QY of the N-*cis* and N-*trans* chromophore are similar, in agreement with our findings of highly dynamic chromophore moieties within the β-barrel structure of rsFolder. Fitting these data to a Henderson–Hasselbalch model yields an apparent pK_a of 5.7 (solid line), 0.25 pH units above the value of 5.45 (dashed line), expected for pH-independent switching rates. Thus, the small, but significant deviation of the measured N-*trans* populations from the simple kinetic model is most likely explained by a pH-dependent $k(\text{tr-cis})_{405}$ switching rate, caused by the transient stabilization of the N-*trans* chromophore by an H-bond to H149 at intermediate pH values. This results in slightly increased N-*trans* populations similar to the observed behavior in the ground state.

The pH dependence of the N-*trans* population under 488 nm illumination (Figure 6b) can be fitted to the same kinetic model (solid line). The fitted "plateau" populations of the N-*trans* state at high (>6) and very low pH (<2) are 0.955 ± 0.005 and 0.55 ± 0.10, respectively. Again, these data provide some insight into the relative switching rates at this wavelength. At acidic pH, we find again similar switching rates, $k(\text{cis-tr})_{488} \approx k(\text{tr-cis})_{488}$, for N-cis and N-trans chromophore species. The significantly increased N-*trans* population at high pH originates from a switching efficiency

https://doi.org/10.1021/jacs.1c02442
J. Am. Chem. Soc. XXXX, XXX, XXX−XXX

$k(\text{cis-tr})_{488}$ that is about 22 times higher for a pure A-*cis* as compared to a pure N-*cis* chromophore state. The apparent pK_a of this pH dependence is 4.0, 1.5 pH units below the ground-state pK_a of the *cis* chromophore. We tentatively assign this large pK_a shift to an increased switching efficiency $k(\text{cis-tr})_{488}$ of the *cis* chromophore species at lower pH that partly compensates for the reduced A-*cis* population. The faster off-switching may be rationalized by a reduced transition state energy in the excited state due to the presence of an increasing amount of H^+ ions.

An important parameter for microscopy applications relying on reversible photoswitching of fluorescent markers is the switching contrast *C*, defined as the ratio of fluorescence measured upon off-to-on switching with 405 nm light and on-to-off switching with 488 nm light. Assuming that only the A-*cis* species is significantly fluorescent, a reduced switching contrast results from the combined effects of residual on-to-off switching by 405 nm light and off-to-on switching by 488 nm light: $C = P(\text{A-}cis)_{405}/P(\text{A-}cis)_{488}$. Figure 6c shows a plot of the pH dependence of the switching contrast as derived from the measured NMR chromophore state populations. Lowering the pH from 8 to 4 results in a reduction of the switching contrast by 1 order of magnitude as a combined effect of the higher amount of *trans* chromophore species present after 405 nm illumination (accounts for a factor of 2) and the lower *cis*-to-*trans* switching efficiency under 488 nm illumination (accounts for a factor of 5). Our NMR-derived results are qualitatively confirmed by ensemble fluorescence measurements (Figure S12) at pH values of 5.4 and 7.3. The slight discrepancy observed between the NMR and fluorescence data mainly arises from the different sample conditions used for these measurements.

CONCLUSION

We have demonstrated that NMR spectroscopy is a powerful tool to differentiate chromophore states in phototransformable fluorescent proteins that may become (simultaneously) populated in solution under a set of experimental conditions (pH, temperature, buffer composition, etc.) either in the dark or under light illumination. The atomic resolution provided by NMR allows to accurately quantify state populations and their interconversion kinetics, adding important information to the static structures obtained from X-ray crystallography. In addition, disentangling the various chromophore states offers a mean of investigating chromophore dynamics, H-bonding to the barrel, on−off switching energy barriers that strongly influence the optical properties of these proteins. For the negative RSFP rsFolder, we could show that the N-*cis* state behaves like a free chromophore in solution that undergoes nonradiative relaxation after light excitation, making it a nonfluorescent species. On the contrary, the A-*cis* chromophore is stabilized by H-bonding to surrounding residues (and a water molecule), which heavily decreases its conformational dynamics, resulting in a 3 orders of magnitude reduction of the chromophore ring flip rate (10 s^{-1} at 40 °C). Although H-bonding interactions with organic chromophores have been reported to induce fluorescence quenching by electron transfer mechanisms,[45] in rsFolder, the NMR-observed conformational stabilization of the A-*cis* chromophore when H-bonded to the β-barrel suggests that H-bonding rather promotes a high fluorescence brightness in fluorescent proteins. Finally, the N-*trans* chromophore shows a pH-dependent stabilization that we have attributed to transient H-bond formation with the imidazoline ring of H149 that is most stable around pH 5. This stabilization significantly modulates *cis*−*trans* isomerization in the dark and also contributes to a reduced switching contrast in fluorescence microscopy. Overall, our data show that the relative populations of fluorescent and nonfluorescent chromophore states vary in a complex pH-dependent manner, with protonation and deprotonation events of the chromophore and nearby residues playing an important role in H-bond dynamics, altering the chromophore's conformational stability and its ability to photoswitch in the dark or under light illumination. We believe that using solution NMR spectroscopy to probe changes in chromophore state populations and dynamics provides a powerful tool to investigate the effects of environmental conditions or protein mutations and to correlate them with altered photophysical properties as a prerequisite for rational design of phototransformable fluorescent protein variants with improved properties.

ASSOCIATED CONTENT

Supporting Information

The Supporting Information is available free of charge at https://pubs.acs.org/doi/10.1021/jacs.1c02442.

Materials and methods (sample preparation and experimental procedures); supplementary figures, presenting additional NMR and absorbance/fluorescence data (PDF)

AUTHOR INFORMATION

Corresponding Author

Bernhard Brutscher − *Univ. Grenoble Alpes, CEA, CNRS, Institut de Biologie Structurale (IBS), 38000 Grenoble, France;* orcid.org/0000-0001-7652-7384; Email: bernhard.brutscher@ibs.fr

Authors

Nina Eleni Christou − *Univ. Grenoble Alpes, CEA, CNRS, Institut de Biologie Structurale (IBS), 38000 Grenoble, France*

Karine Giandoreggio-Barranco − *Univ. Grenoble Alpes, CEA, CNRS, Institut de Biologie Structurale (IBS), 38000 Grenoble, France*

Isabel Ayala − *Univ. Grenoble Alpes, CEA, CNRS, Institut de Biologie Structurale (IBS), 38000 Grenoble, France*

Oleksandr Glushonkov − *Univ. Grenoble Alpes, CEA, CNRS, Institut de Biologie Structurale (IBS), 38000 Grenoble, France*

Virgile Adam − *Univ. Grenoble Alpes, CEA, CNRS, Institut de Biologie Structurale (IBS), 38000 Grenoble, France;* orcid.org/0000-0003-2209-7846

Dominique Bourgeois − *Univ. Grenoble Alpes, CEA, CNRS, Institut de Biologie Structurale (IBS), 38000 Grenoble, France;* orcid.org/0000-0002-1862-7712

Complete contact information is available at: https://pubs.acs.org/10.1021/jacs.1c02442

Notes

The authors declare no competing financial interest.

ACKNOWLEDGMENTS

Financial support from the CNRS (Défis Instrumentation 2018 grant), iNEXT-Discovery, project number 871037, funded by the Horizon 2020 program of the European Commission, and

the Agence Nationale de la Recherche (grants ANR-17-CE11-0047-01 and ANR-20-CE11-0013-01 to D.B.) is acknowledged. This work used the NMR and isotope labeling platforms of the Grenoble Instruct-ERIC center (ISBG; UMS 3518 CNRS-CEA-UJF-EMBL) within the Grenoble Partnership for Structural Biology (PSB). Platform access was supported by FRISBI (ANR-10-INBS-05-02) and GRAL, a project of the University Grenoble Alpes graduate school (Ecoles Universitaires de Recherche) CBH-EUR-GS (ANR-17-EURE-0003). IBS acknowledges integration into the Interdisciplinary Research Institute of Grenoble (IRIG, CEA). We thank Dr. Paul Schanda for stimulating discussions and for contributing a script for the analysis of EXSY data.

REFERENCES

(1) Nienhaus, K.; Nienhaus, G. U. Fluorescent Proteins for Live-Cell Imaging with Super-Resolution. *Chem. Soc. Rev.* **2014**, *43*, 1088−1106.
(2) Querard, J.; Zhang, R.; Kelemen, Z.; Plamont, M.-A.; Xie, X.; Chouket, R.; Roemgens, I.; Korepina, Y.; Albright, S.; Ipendey, E.; Volovitch, M.; Sladitschek, H. L.; Neveu, P.; Gissot, L.; Gautier, A.; Faure, J.-D.; Croquette, V.; Le Saux, T.; Jullien, L. Resonant Out-of-Phase Fluorescence Microscopy and Remote Imaging Overcome Spectral Limitations. *Nat. Commun.* **2017**, *8* (969), 969.
(3) Vetschera, P.; Mishra, K.; Fuenzalida-werner, J. P.; Chmyrov, A.; Ntziachristos, V.; Stiel, A. C. Characterization of Reversibly Switchable Fluorescent Proteins in Optoacoustic Imaging. *Anal. Chem.* **2018**, *90*, 10527−10535.
(4) Chirgwandi, Z. G.; Panas, I.; Johansson, L. G.; Norden, B.; Willander, M.; Winkler, D.; Agren, H. Properties of a Biophotovoltaic Nanodevice. *J. Phys. Chem. C* **2008**, *112*, 18717−18721.
(5) Adam, V.; Mizuno, H.; Grichine, A.; Hotta, J.; Yamagata, Y.; Moeyaert, B.; Nienhaus, G. U.; Miyawaki, A.; Bourgeois, D.; Hofkens, J. Data Storage Based on Photochromic and Photoconvertible Fluorescent Proteins. *J. Biotechnol.* **2010**, *149* (4), 289−298.
(6) Bourgeois, D.; Adam, V.; Fourier, J. Critical Review Reversible Photoswitching in Fluorescent Proteins : A Mechanistic View. *IUBMB Life* **2012**, *64*, 482−491.
(7) Ando, R.; Flors, C.; Mizuno, H.; Hofkens, J.; Miyawaki, A. Highlighted Generation of Fluorescence Signals Using Simultaneous Two-Color Irradiation on Dronpa Mutants. *Biophys. J.* **2007**, *92* (12), L97−L99.
(8) Ando, R.; Mizuno, H.; Miyawaki, A. Regulated Fast Nucleocytoplasmic Shuttling Observed by Reversible Protein Highlighting. *Science (Washington, DC, U. S.)* **2004**, *306* (5700), 1370−1373.
(9) Brakemann, T.; Stiel, A. C.; Weber, G.; Andresen, M.; Testa, I.; Grotjohann, T.; Leutenegger, M.; Plessmann, U.; Urlaub, H.; Eggeling, C.; Wahl, M. C.; Hell, S. W.; Jakobs, S. A Reversibly Photoswitchable GFP-like Protein with Fluorescence Excitation Decoupled from Switching. *Nat. Biotechnol.* **2011**, *29* (10), 942−947.
(10) Grotjohann, T.; Testa, I.; Reuss, M.; Brakemann, T.; Eggeling, C.; Hell, S. W.; Jakobs, S. RsEGFP2 Enables Fast RESOLFT Nanoscopy of Living Cells. *eLife* **2012**, *1*, e00248.
(11) El Khatib, M.; Martins, A.; Bourgeois, D.; Colletier, J.-P.; Adam, V. Rational Design of Ultrastable and Reversibly Photoswitchable Fluorescent Proteins for Super-Resolution Imaging of the Bacterial Periplasm. *Sci. Rep.* **2016**, *6*, 18459.
(12) Wu, L.; Burgess, K. Syntheses of Highly Fluorescent GFP-Chromophore Analogues. *J. Am. Chem. Soc.* **2008**, *130*, 4089−4096.
(13) Megley, C. M.; Dickson, L. A.; Maddalo, S. L.; Chandler, G. J.; Zimmer, M. Photophysics and Dihedral Freedom of the Chromophore in Yellow, Blue, and Green Fluorescent Protein. *J. Phys. Chem. B* **2009**, *113* (1), 302−308.
(14) Niwa, H.; Inouye, S.; Hirano, T.; Matsuno, T.; Kojima, S.; Kubota, M.; Ohashi, M.; Tsuji, F. Chemical Nature of the Light Emitter of the Aequorea Green Fluorescent Protein. *Proc. Natl. Acad. Sci. U. S. A.* **1996**, *93*, 13617−13622.
(15) Weber, W.; Helms, V.; McCammon, J. A.; Langhoff, P. Shedding Light on the Dark and Weakly Fluorescent States of Green Fluorescent Proteins. *Proc. Natl. Acad. Sci. U. S. A.* **1999**, *96* (May), 6177−6182.
(16) Follenius-Wund, A.; Bourotte, M.; Schmitt, M.; Iyice, F.; Lami, H.; Bourguignon, J.-J.; Haiech, J.; Pigault, Cl. Fluorescent Derivatives of the GFP Chromophore Give a New Insight into the GFP Fluorescence Process. *Biophys. J.* **2003**, *85* (3), 1839−1850.
(17) De Zitter, E.; Ridard, J.; Thedie, D.; Adam, V.; Levy, B.; Byrdin, M.; Gotthard, G.; Van Meervelt, L.; Dedecker, P.; Demachy, I.; Bourgeois, D. Mechanistic Investigations of Green MEos4b Reveal a Dynamic Long-Lived Dark State. *J. Am. Chem. Soc.* **2020**, *142*, 10978−10988.
(18) Andresen, M.; Stiel, A. C.; Trowitzsch, S.; Weber, G.; Eggeling, C.; Wahl, M. C.; Hell, S. W.; Jakobs, S. Structural Basis for Reversible Photoswitching in Dronpa. *Proc. Natl. Acad. Sci. U. S. A.* **2007**, *104* (32), 13005−13009.
(19) Shinoda, H.; Lu, K.; Nakashima, R.; Wazawa, T.; Noguchi, K.; Matsuda, T.; Nagai, T. Acid-Tolerant Reversibly Switchable Green Fluorescent Protein for Super-Resolution Imaging under Acidic Conditions Resource Acid-Tolerant Reversibly Switchable Green Fluorescent Protein for Super-Resolution Imaging under Acidic Conditions. *Cell Chem. Biol.* **2019**, *26*, 1−11.
(20) Takaba, K.; Tai, Y.; Eki, H.; Dao, H.; Hanazono, Y.; Hasegawa, K.; Miki, K.; Takeda, K. Subatomic Resolution X-Ray Structures of Green Fluorescent Protein. *IUCrJ.* **2019**, *6*, 387−400.
(21) Laptenok, S. P.; Gil, A. A.; Hall, C. R.; Lukacs, A.; Iuliano, J. N.; Jones, G. A.; Greetham, G. M.; Donaldson, P.; Miyawaki, A.; Tonge, P. J.; Meech, S. R. Infrared Spectroscopy Reveals Multi-Step Multi-Timescale Photoactivation in the Photoconvertible Protein Archetype Dronpa. *Nat. Chem.* **2018**, *10*, 845−852.
(22) Warren, M. M.; Kaucikas, M.; Fitzpatrick, A.; Champion, P.; Sage, J. T.; van Thor, J. J. Ground-State Proton Transfer in the Photoswitching Reactions of the Fluorescent Protein Dronpa. *Nat. Commun.* **2013**, *4*, 1461−1468.
(23) Christou, N.-E.; Ayala, I.; Giandoreggio-barranco, K.; Byrdin, M.; Adam, V.; Bourgeois, D.; Brutscher, B. NMR Reveals Light-Induced Changes in the Dynamics of a Photoswitchable Fluorescent Protein. *Biophys. J.* **2019**, *117* (11), 2087−2100.
(24) Jensen, N. A.; Jansen, I.; Kamper, M.; Jakobs, S. Reversibly Switchable Fluorescent Proteins for RESOLFT Nanoscopy. In *Nanoscale Photonic Imaging*; Springer International Publishing: 2020; pp 241−261.
(25) Abbandonato, G.; Signore, G.; Nifosi, R.; Voliani, V.; Bizzarri, R.; Beltram, F. Cis − Trans Photoisomerization Properties of GFP Chromophore Analogs. *Eur. Biophys. J.* **2011**, *40*, 1205−1214.
(26) Voliani, V.; Bizzarri, R.; Nifosı, R.; Abbruzzetti, S.; Grandi, E.; Viappiani, C.; Beltram, F. Cis - Trans Photoisomerization of Fluorescent-Protein Chromophores. *J. Phys. Chem. B* **2008**, *112*, 10714−10722.
(27) Loria, J. P.; Rance, M.; Palmer, A. G. A Relaxation-Compensated Carr - Purcell - Meiboom - Gill Sequence for Characterizing Chemical Exchange by NMR Spectroscopy. *J. Am. Chem. Soc.* **1999**, *121* (16), 2331−2332.
(28) Franco, R.; Gil-Caballero, S.; Ayala, I.; Favier, A.; Brutscher, B. Probing Conformational Exchange Dynamics in a Short-Lived Protein Folding Intermediate by Real-Time Relaxation-Dispersion NMR. *J. Am. Chem. Soc.* **2017**, *139* (3), 1065−1068.
(29) Shinobu, A.; Agmon, N. The Hole in the Barrel : Water Exchange at the GFP Chromophore. *J. Phys. Chem. B* **2015**, *119*, 3464−3478.
(30) Regmi, C. K.; Bhandari, Y. R.; Gerstman, B. S.; Chapagain, P. P. Exploring the Diffusion of Molecular Oxygen in the Red Fluorescent Protein MCherry Using Explicit Oxygen Molecular Dynamics Simulations. *J. Phys. Chem. B* **2013**, *117* (8), 2247−2253.
(31) Mallik, R.; Udgaonkar, J. B.; Krishnamoorthy, G. Kinetics of Proton Transfer in a Green Fluorescent Protein: A Laser-Induced PH

https://doi.org/10.1021/jacs.1c02442
J. Am. Chem. Soc. XXXX, XXX, XXX−XXX

Jump Study. *Proc. - Indian Acad. Sci., Chem. Sci.* **2003**, *115* (4), 307−317.
(32) Saxena, A. M.; Udgaonkar, J. B.; Krishnamoorthy, G. Protein Dynamics Control Proton Transfer from Bulk Solvent to Protein Interior: A Case Study with a Green Fluorescent Protein. *Protein Sci.* **2005**, *14* (7), 1787−1799.
(33) Agmon, N. Proton Pathways in Green Fluorescence Protein. *Biophys. J.* **2005**, *88* (4), 2452−2461.
(34) Shinobu, A.; Agmon, N. Proton Wire Dynamics in the Green Fluorescent Protein. *J. Chem. Theory Comput.* **2017**, *13* (1), 353−369.
(35) Weininger, U.; Modig, K.; Akke, M. Ring Flips Revisited: 13 C Relaxation Dispersion Measurements of Aromatic Side Chain Dynamics and Activation Barriers in Basic Pancreatic Trypsin Inhibitor. *Biochemistry* **2014**, *53*, 4519−4525.
(36) Montelione, G. T.; Wagner, G. 2D Chemical Exchange NMR Spectroscopy by Proton-Detected Heteronuclear Correlation. *J. Am. Chem. Soc.* **1989**, *111* (6), 3096−3098.
(37) Woodhouse, J.; Nass Kovacs, G.; Coquelle, N.; Uriarte, L. M.; Adam, V.; Barends, T. R. M.; Byrdin, M.; de la Mora, E.; Bruce Doak, R.; Feliks, M.; Field, M.; Fieschi, F.; Guillon, V.; Jakobs, S.; Joti, Y.; Macheboeuf, P.; Motomura, K.; Nass, K.; Owada, S.; Roome, C. M.; Ruckebusch, C.; Schiro, G.; Shoeman, R. L.; Thepaut, M.; Togashi, T.; Tono, K.; Yabashi, M.; Cammarata, M.; Foucar, L.; Bourgeois, D.; Sliwa, M.; Colletier, J.-P.; Schlichting, I.; Weik, M. Photoswitching Mechanism of a Fluorescent Protein Revealed by Time-Resolved Crystallography and Transient Absorption Spectroscopy. *Nat. Commun.* **2020**, *11*, 741.
(38) Abbruzzetti, S.; Grandi, E.; Viappiani, C.; Bologna, S.; Campanini, B.; Raboni, S.; Bettati, S.; Mozzarelli, A. Kinetics of Acid-Induced Spectral Changes in the GFPmut2 Chromophore. *J. Am. Chem. Soc.* **2005**, *127* (13), 626−635.
(39) Gayda, S.; Nienhaus, K.; Nienhaus, G. U. Mechanistic Insights into Reversible Photoactivation in Proteins of the GFP Family. *Biophys. J.* **2012**, *103* (12), 2521−2531.
(40) Platzer, G.; Okon, M.; Mcintosh, L. P. PH-Dependent Random Coil 1H, 13C, and 15N Chemical Shifts of the Ionizable Amino Acids : A Guide for Protein PKa Measurements. *J. Biomol. NMR* **2014**, *60*, 109−129.
(41) Pletnev, S.; Shcherbo, D.; Chudakov, D. M.; Pletneva, N.; Merzlyak, E. M.; Wlodawer, A.; Dauter, Z.; Pletnev, V. A Crystallographic Study of Bright Far-Red Fluorescent Protein MKate Reveals PH-Induced Cis-Trans Isomerization. *J. Biol. Chem.* **2008**, *283* (43), 28980−28987.
(42) Violot, S.; Carpentier, P.; Blanchoin, L.; Bourgeois, D. Reverse PH-Dependence of Chromophore Protonation Explains the Large Stokes Shift of the Red Fluorescent Protein MKeima. *J. Am. Chem. Soc.* **2009**, *131* (30), 10356−10357.
(43) Pace, C. N.; Fu, H.; Fryar, K. L.; Landua, J.; Trevino, S. R.; Schell, D.; Thurlkill, R. L.; Imura, S.; Scholtz, J. M.; Gajiwala, K.; Sevcik, J.; Urbanikova, L.; Myers, J. K.; Takano, K.; Hebert, E. J.; Shirley, B. A.; Grimsley, G. R. Contribution of Hydrogen Bonds to Protein Stability. *Protein Sci.* **2014**, *23*, 652−661.
(44) Gao, J.; Bosco, D. A; Powers, E. T; Kelly, J. W Localized Thermodynamic Coupling between Hydrogen Bonding and Microenvironment Polarity Substantially Stabilizes Proteins. *Nat. Struct. Mol. Biol.* **2009**, *16* (7), 684−690.
(45) Zhao, G. J.; Liu, J. Y.; Zhou, L. C.; Han, K. L. Site-Selective Photoinduced Electron Transfer from Alcoholic Solvents to the Chromophore Facilitated by Hydrogen Bonding: A New Fluorescence Quenching Mechanism. *J. Phys. Chem. B* **2007**, *111* (30), 8940−8945.

https://doi.org/10.1021/jacs.1c02442
J. Am. Chem. Soc. XXXX, XXX, XXX−XXX